Hindawi
International Journal of Energy Research
Volume 2024, Article ID 5513198, 15 pages
https://doi.org/10.1155/2024/5513198

Research Article

Comparative Analysis of Reverse Truncated Pyramid and Other Nonimaging Concentrators as the Receiver in Laser Wireless Power Transmission System

Xian-long Meng,[1,2] **Xin-yuan Li**,[1,2] **Yi-chao Hou**,[1,2] **Pu Zhang**,[1,2] **and Cun-liang Liu**[1,2]

[1]*School of Power and Energy, Northwestern Polytechnical University, 1 Dongxiang Road, Chang'an District, Xi'an, Shaanxi 710072, China*
[2]*Shaanxi Key Laboratory of Thermal Sciences in Aero-engine System, Northwestern Polytechnical University, Xi'an, Shaanxi 710129, China*

Correspondence should be addressed to Cun-liang Liu; liucunliang@nwpu.edu.cn

Received 10 December 2023; Revised 28 February 2024; Accepted 4 April 2024; Published 2 May 2024

Academic Editor: Koteswara Raju Dhenuvakonda

The global energy landscape faces significant challenges in meeting the demands of modern industries for stable and efficient energy supply. Laser wireless power transmission (LWPT) systems, which utilize the photovoltaic effect to convert laser beam energy, hold great promise due to their long-range transmission capability and high precision. However, the current energy conversion efficiency of these systems requires further improvement to achieve optimal performance. To enhance concentrated photovoltaic (CPV) system performance, the study examines different nonimaging concentrators such as reverse truncated pyramid, cross-compound parabolic concentrator, and square elliptical hyperboloid. Numerical simulations using the finite element method analyze the multifield coupling mechanism of PV modules with various concentration lenses. Three CPV systems with RTP concentrators of different heights were studied to understand the impact of geometry on CPV performance. And the main impact of rotation angle was discussed. The research findings provide essential insights into CPV system performance and the influence of different concentration lenses, contributing valuable knowledge towards improving LWPT technologies.

1. Introduction

The global energy issue has become a significant factor hindering human development. Ensuring a stable and reliable energy supply represents a major challenge faced by modern industries. Conventional wired energy transfer methods suffer from various limitations, particularly in terms of security and mobility aspects [1]. In contrast, the laser wireless power transmission (LWPT) system, which capitalizes on the photovoltaic effect to convert laser beam energy during transmission, presents noteworthy advantages, including long-range transmission capability and high precision [2]. LWPT finds wide applications in medium- and long-distance power transmission scenarios, distinguishing it from other wireless transmission technologies like electromagnetic induction and magnetic field resonance coupling [3]. The vast application potential of LWPT lies in the ground, space to ground, and space-based practical applications [4, 5].

Despite the clear benefits of using LWPT technology, it also has drawbacks that hinder the optimal performance and efficiency compared to other types of energy transmission. Currently, the overall efficiency of LWPT systems is quite low (around 20% or less) [2, 6]. The main technical challenge lies in developing a high-power laser emitter and improving the conversion efficiency of the receiver. Under the middle/far transmission range, the receiving heat flux presents a fluctuating, nonuniform distribution, which is considered the main reason for the drop in efficiency

[7–9]. Maintaining the divergence of the laser beam is crucial to prevent a drop in energy conversion efficiency due to misalignment between the laser and the receiver [10]. For a moving LWPT receiver, a tracking device similar to solar tracking is required for the laser emitter. Furthermore, laser power transmission attenuation occurs when the laser power decreases along its transmission path through clouds, polluted air with dust, and other obstacles, with the degree of attenuation dependent on these factors [11].

Concentrated photovoltaics (CPV) is a technology that allows concentrating irradiation on a small surface area of a photovoltaic cell. CPV systems use low-cost optical devices with large surface areas, including lenses and mirrors with curved surfaces, to collect as many beams as possible on the small PV cell surface area, achieving the highest module efficiency [12, 13]. CPV systems not only reduce the space occupied by PV elements but also aim to achieve higher performance by substituting expensive materials with cheaper alternatives, thereby reducing the total cost of the element [14]. Therefore, the receiving part of LWPT system specifically with beam collector or lens is worthy of research and still requires improvement [15]. The geometry of the beam collector needs to be rearranged to collect more beams from the source and minimize nonuniform irradiation. Nonimaging optical devices, such as the compound parabolic concentrator (CPC) or cross-compound parabolic concentrator (CCPC), can enlarge the acceptance angle to receive more rays from different incident ray vectors [16, 17]. The reverse truncated pyramid (RTP) geometry was an alternative geometry used as a secondary optic element in solar energy applications before. The RTP concentrator has a right pyramid geometry that is truncated at the base to match the size of the PV cell, with a trapezoidal cross-section [18]. Unlike a CCPC, the geometrical concentration ratio of RTP is not constrained and may have any value. RTP lenses are generally made of glass or transparent polymer, and the walls can be covered with a thin layer of aluminum with reflectivity over 90%. RTP lenses have been successfully used by companies like Amonix in CPV systems, achieving performance equal to 35.9% according to NREL [19]. Although RTP geometry is considered less sophisticated compared to CCPC, it is the easiest and cheapest to manufacture on a large scale and is frequently used in different CPV systems [20]. The only drawback of using multiple RTP lenses in one system is the overall optical efficiency drop corresponding to the quantity of RTP units; the more lenses used, the more optical losses occur [21].

The efficiency of CPV systems is mainly determined by the receiver performance, making the use of optical concentrator much potential to the improvement of output efficiency. The PV receiver can be projected to meet specific requirements, with the shape and dimensions modified to best match the working conditions, laser characteristics, and other parameters if necessary. The use of concentrators in combination with PV cells should increase the system's efficiency, compensating for inaccuracies and tracking errors to prevent a drop in performance to zero [22]. The present study is aimed at investigating the multifield coupling performance of CPV receivers using the reverse truncated pyramid (RTP) concentrator and comparing it with other nonimaging concentrators, such as cross-compound parabolic concentrator (CCPC) and square elliptical hyperboloid (SEH), in laser wireless power transmission systems. Improved conversion efficiency of the LWPT system is expected with enhancements to the receiving part. It is essential to note that the LWPT system significantly differs from conventional concentrated solar energy systems due to its operation with high-density beams, where system efficiency hinges on the successful construction of a receiver that ensures stable radiation heat transfer and photoelectric mechanisms. The paper employs the finite element method for numerical simulation and analysis of the PV module's multifield coupling mechanism with different concentration lenses. Experimental setups are utilized to assess the crucial characteristics of the PV module under nonuniform illumination. The research outcomes provide valuable insights into the performance of various concentration lenses for CPV systems.

2. Modelling

The process of remote laser power transfer was reconstructed and studied using the FEM software COMSOL Multiphysics. The laser wireless power transmission (LWPT) system comprises several crucial elements. Firstly, there is the laser source, which emits a set of beams with the same frequency and power, distributed according to the Gaussian law. The second element is the PV cell, serving as the receiver of monochromatic light. The PV cell is positioned in space with its front surface and contacts directed towards the laser source. Between the laser emitter and the PV cell, there is an irradiation concentrator, which rearranges the beam distribution to the PV cell, aiming to make it as uniform as possible.

For the simulation, three designs of concentrators were considered: the reverse truncated pyramid (RTP) concentrator, the conventional cross-compound parabolic concentrator (CCPC), and the square elliptic hyperboloid (SEH) concentrator (Figure 1). The simulated system includes three concentrators (CCPC, SEH, and RTP) made of polymethylmethacrylate, one filling made of Sylgard 165, one silicon wafer, one metallic busbar, and four metallic fingers.

The simulation incorporates combined electric, optical, and heat transfer physics, and it consists of two study chapters: a stationary study that solves electrical, optical, and heat transfer equations and a ray-tracing study that provides data on the heat flux distribution and the scheme of ray paths. By using this simulation approach, the multifield coupling effects of different concentrators in the LWPT system can be thoroughly investigated and understood.

2.1. Optical Model

2.1.1. Laser Source. The laser beam modeled in the software should accurately replicate the characteristics of the laser used in the experimental evaluation, such as the BWT Beijing DS3-51512 laser machine, to ensure consistency and reliability. In the FEM software, the key parameters of the laser beam, including the divergence angle (β), wavelength (λ), and Gaussian distribution of power, are precisely set.

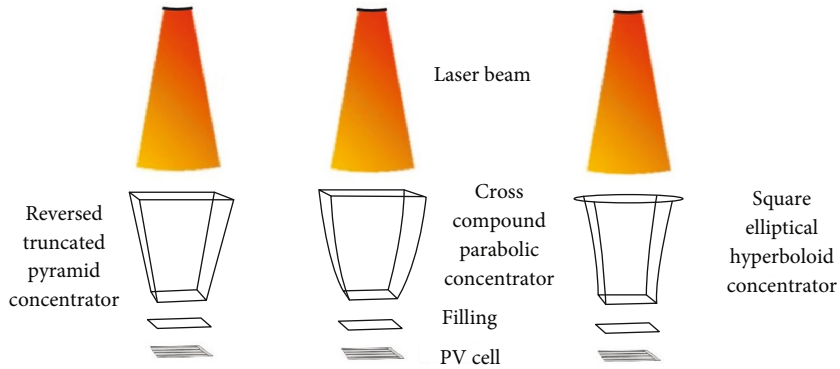

Figure 1: Main elements of modelling.

Figure 2 illustrates the scheme of the Gaussian intensity distribution of the laser beam, while Figure 3 presents the 2-D model of the laser spot with the Gaussian power distribution. These representations help visualize the spatial distribution of the laser's intensity across the target surface. By accurately modelling the laser beam's characteristics, such as divergence, wavelength, and power distribution, the FEM software allows for a comprehensive analysis of the laser's behavior and its interaction with the target, enabling valuable insights into the laser power transmission process and its impact on the receiver's performance.

The propagation of the laser beam is characterized by the wavefront's radius of curvature at different z coordinates, measured in meters (m). This radius of curvature represents the curvature of the wavefront at a given distance along the z-axis and is a crucial parameter in describing the behavior of the laser beam during its propagation:

$$R(z) = z\left[1 + \left(\frac{\pi w_0^2}{\lambda_z}\right)^2\right]. \quad (1)$$

The beam radius at z coordinate $w(z)$(m) is as follows:

$$w(z) = w_0\left[1 + \left(\frac{\lambda_z}{\pi w_0^2}\right)^2\right]^{1/2}, \quad (2)$$

where z is the distance from the plane with flat wavefront (m), λ_z is the wavelength of the beam (m), and w_0 is the beam waist (m).

The irradiance distribution of Gaussian beam is determined by the following equation:

$$I(r) = I_0 e^{-2r^2/w^2} = \frac{2P}{\pi w^2} e^{-2r^2/w^2}, \quad (3)$$

where $w = w(z)$ and P is the total power of the beam (W).

One more characteristic of the beam shape is divergence half-angle (β), that is, angle between the axis of beam propagation and line of asymptotic cone.

The value of divergence half-angle (β) (rad) is determined by the following equation:

$$\sin(\beta) = \frac{w(z)}{z} = \frac{\lambda}{\pi w_0}. \quad (4)$$

The FEM software allows users to configure the release of the laser beam from any point in space with a specified divergence angle (β) by defining the x, y, and z coordinates. For the geometrical optic part of the simulation, the wavelength (λ) of the released rays was set to 808 nm. The position of the laser source in space and its direction were determined based on the spatial coordinates of the beam waist and the coordinates of the beam vector. The beam waist was positioned at a distance "d" along the z-axis and directed downward perpendicular to the surface of the PV cell. The laser beam type was set as a point source, with a total of 200 rays released from the point. The beam divergence half-angle (β) was chosen to be 0.001 rad. Additionally, the total encircled power of the laser was set to 1 W. These settings in the FEM software accurately represent the geometrical and power characteristics of the laser during the simulation.

2.1.2. Concentrating Element. In the FEM simulation, a total of 6 models were created, consisting of 3 different types of secondary concentrators. Among these models, there was one cross-compound parabolic concentrator, two square elliptical hyperboloids, and three reversed truncated pyramids. Each of these concentrator models had unique dimensions.

All the concentrators in the simulation were designed with transparent entrance apertures and fully reflective side walls, meaning that they had an absorption coefficient (α) of 0. Additionally, these concentrators were constructed using polymethyl methacrylate (PMMA) as the material.

The optical properties of PMMA and other materials used in the construction of CPV system elements were specified and are provided in Table 1. These properties play a crucial role in the behavior and performance of the concentrators and overall CPV system during the simulation.

The geometry used in the simulation represents a cropped pyramid, known as the reversed truncated pyramid (RTP) concentrator. This concentrator has square entrance and exit apertures of different areas. All sides of the pyramid

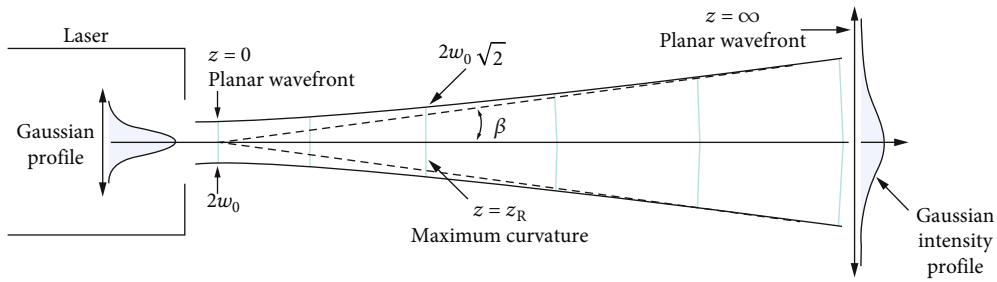

Figure 2: Gaussian beam intensity distribution [23].

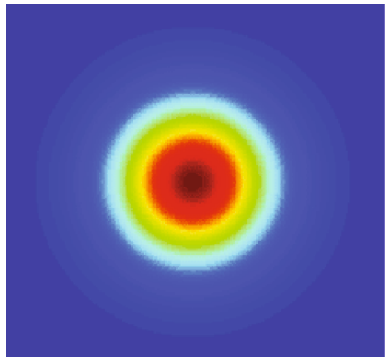

Figure 3: Gaussian distribution laser spot.

Table 1: Optical properties of domains.

Component	Material	Refractive index n
Busbar	Copper	0.25598
Finger	Copper	0.25598
Wafer	Silicon	3.674
Filling	Sylgard 165	1.4
Concentrator	PMMA	1.5

have a flat form and are symmetrical to the opposite side. The dimensions of the concentrator are characterized by three parameters: the width of the bottom aperture (W), the height of the concentrator (H), and the inclination angle of the side wall (α).

$$\frac{W}{H} = -(\tan 2\alpha + \cos \alpha), \tag{5}$$

where α is the angle between the side wall and the basement plane (degree), W is the width of base aperture (m), and H is the height concentrator (m).

The conventional design of the RTP concentrator ensures efficient concentration and redirection of light towards the PV cell, maximizing the overall performance of the concentrator in the CPV system. In the current simulations, the length of the top and bottom apertures of the reversed truncated pyramid (RTP) concentrator was set to be equal to 19 mm and 10 mm, respectively, resulting in a concentration ratio (Cg) of 3.6. The three different geometries of the RTP concentrator were distinguished solely by the value of the height (H), which were 6 mm, 16 mm, and 25 mm. These variations in height allow for the investigation of different concentrator configurations and their impact on the performance of the laser wireless power transmission (LWPT) system when used as receivers in CPV applications.

2.1.3. Optical Efficiency and Influence of Rotation. The important characteristic of any type of concentrator is optical efficiency (η_{opt}). It is performed by the ratio of the number of rays that passed through the optical aperture ($P_{aperture}$) to the number of rays that reached the surface of PV element ($P_{flux\ cell}$) [24]:

$$\eta = \frac{P_{flux\ cell}}{P_{aperture}}. \tag{6}$$

In the current model, a set of rays is released from a point in space and shaped as a cone, reaching the entrance aperture of the receiver. The laser emitter remains fixed in space and maintains a constant divergence angle for all studied geometries. To assess the performance of the laser wireless power transmission (LWPT) system, the receiving part, comprising the concentrator, PV cell, and filling material, is rotated around an axis passing through the center of opposite sides that form the top aperture, at various angles (θ) (see Figure 4). The angle values range from 0° to 50° with a step of 10°.

For each of the six geometries, all parameters of the concentrated photovoltaic (CPV) system, including optical, electrical, and heat parameters, were studied at 0° rotation angle and then repeated at 10°, 20°, 30°, 40°, and 50° angles. These comprehensive simulations provide insights into the behavior and performance of the LWPT system under various conditions, offering valuable information for optimizing and enhancing its efficiency.

2.2. Electrical Model. The electrical model of the PV cell is based on the classical single diode photovoltaic cell, as illustrated in Figure 5. This model is commonly used to describe the behavior of PV cells and is widely accepted for simulating their electrical characteristics. It includes a single diode to represent the junction between the p-type and n-type semiconductors in the PV cell. The diode allows the current to flow in only one direction, representing the generation of electricity when the cell is exposed to light.

By using this electrical model, we can simulate the behavior of the PV cell under different operating conditions and illumination levels. This enables us to study the

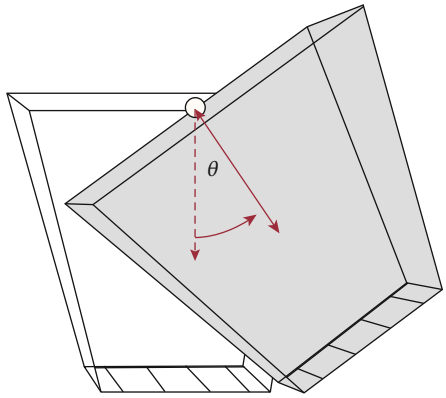

Figure 4: General sketch of CPV system with rotation.

electrical performance and efficiency of the PV cell in the laser wireless power transmission (LWPT) system and analyze its response to various parameters, such as incident light intensity, temperature, and structural design.

I-V characteristics of PV cell under irradiance is equal to difference of independent current generated by the internal photoelectrical effect and dark current:

$$I = I_{\mathrm{p}} - I_{\mathrm{dc}}, \tag{7}$$

where I is the total current in external load R_{s} (A), I_{p} is the current generated by incident photons (A), and I_{dc} is the dark current (A).

The total current flow of the PV cell under illumination can be described by the following equation:

$$I = I_{\mathrm{p}} - I_0\left[e^{(V+R_sI)/nV_{\mathrm{T}}} - 1\right] - \frac{V + R_{\mathrm{s}}I}{R_{\mathrm{sh}}}, \tag{8}$$

where I_0 is the diode reverse saturation current (A), n is the ideality factor (1), R_{s} is the series resistance (ohm), R_{sh} is the shunt resistance (ohm), V is the average cell voltage (V), and V_{T} is the thermodynamic voltage.

The resistances R_{s} and R_{sh} are parasitic elements and reflect the imperfections in the behavior of real PV element. Thermodynamic voltage is expressed by the following equation:

$$V_{\mathrm{T}} = \frac{kT}{e}, \tag{9}$$

where k is the Boltzmann constant (J/K), T is the photovoltaic cell temperature (K), and e is the charge of electron (C).

Photocurrent is taken as proportional to the intensity of incident light (G).

$$I_p \sim G. \tag{10}$$

Considering the current generated in both illuminated and dark regions of PV cell can be written the resulting equation for the current of entire PV cell:

$$I = C_1G + C_2T^3e^{(-T_1/T)}\left[e^{(V_1/nV_T)} - 1\right] + C_3V_1, \tag{11}$$

where C_1 is the multivariable regression coefficient (A/W), C_2 is the multivariable regression coefficient (A/m^{2}K^3), C_3 is the multivariable regression coefficient (A/m^{2}V), G is the intensity of irradiation (W/m^2), T_1 is the diode temperature (K), and V_1 is the diode voltage (V).

$$V_1 = V + R_{\mathrm{s}}I. \tag{12}$$

After the coefficients C_1, C_2, and C_3 are received, the resistance R_{s} and ideality factor n are selected to get the best suited coefficients of determination. This action is repeated till the parameters become similar. One more parameter that displays the quality of PV system is fill factor. It is defined by the following equation:

$$\mathrm{FF} = \frac{P_{\mathrm{m}}}{V_{\mathrm{oc}}I_{\mathrm{sc}}}, \tag{13}$$

where P_{m} is the peak power (W), V_{oc} is the open-circuit voltage (V), and I_{sc} is the short-circuit current (A).

The fill factor value commonly lies in the range from 0.5 to 0.82 [4, 25].

The electrical model of the PV cell in this study incorporates a silicon wafer, four fingers, and a busbar, all made of copper. The stationary study includes a set of boundary conditions to accurately simulate the electrical behavior of the PV cell.

The external edges of the PV cell system are electrically insulated, which means that no current can flow in or out through these edges. On the internal edges, there is no generation of the current between the illuminated region (where the incident light falls) and the dark region (where there is no incident light). At the edges of the busbar, an electrical potential V0 is created. The values of the electrical potential V0 are selected from a range of 0 to 0.64 V. By varying the electrical potential values, the behavior of the PV cell under different external biases can be investigated. This allows for a comprehensive analysis of the electrical characteristics and performance of the PV cell in the LWPT system.

2.3. Heat Transfer Model. The current model incorporates heat conduction and convection heat flux to interact with the surrounding medium. To determine the values of heat flux for the PV cell system with concentrator, a specific set of boundary conditions was defined to describe how the system interacts with the surrounding medium. These boundary conditions were applied to certain faces of the geometry, and the heat flux can be defined by the following equation:

$$q = -k \cdot \nabla T + h \cdot \left(T_{\mathrm{pv\,cell}} - T_{\infty}\right), \tag{14}$$

where T_{∞} is the surrounding temperature (K), $T_{\mathrm{pv\,cell}}$ is the PV cell temperature (K), k is the thermal conductivity of material (W/m•K), h is the heat transfer coefficient (W/m^2•K), and q is the heat flux from boundary (W/m^2).

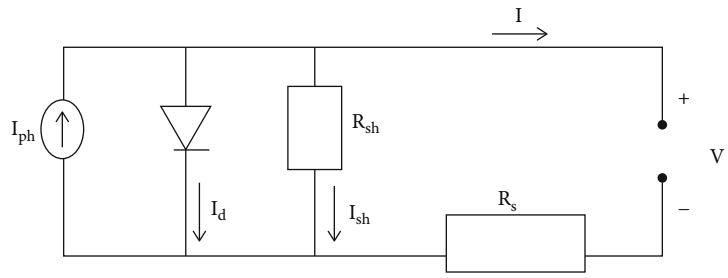

Figure 5: Equivalent circuit for PV cell [25, 26].

The external medium's temperature was set at 293.15 K. The side walls and top surface of the concentrator interact with the medium through heat convection with a heat transfer coefficient of $h = 50\,\mathrm{W/(m^2{\cdot}K)}$. The base surface of the PV cell transfers heat through convection as well, with a heat transfer coefficient of $150\,\mathrm{W/(m^2{\cdot}K)}$.

In this model, the PV cell is considered as the source of heat. The "electromagnetic heating" multiphysics coupling is applied to the PV cell, as direct current flows through the conductor, leading to the release of heat according to the Joule-Lenz law. The heat is then transferred inside the PV cell to its boundaries through heat conduction. This heat conduction process can be described by the steady heat conduction equation:

$$\frac{\partial}{\partial x}\left(k\frac{\partial T}{\partial x}\right) + \frac{\partial}{\partial y}\left(k\frac{\partial T}{\partial y}\right) + \frac{\partial}{\partial z}\left(k\frac{\partial T}{\partial z}\right) + \dot{q}_r = \rho c\frac{\partial T}{\partial t}, \quad (15)$$

where $\dot{q}_r$ is the residual energy (W), ρ is the density ($\mathrm{kg/m^3}$), and c is the heat capacity (J/m•K).

The residual heat energy of the laser beam refers to the amount of laser energy that is not converted into electrical current and remains as heat. This heat is transferred inside the PV cell through conduction and is defined as a heat source on the top surface of the PV cell. The dissipation of this heat from the boundary is modeled by convection and is solved using equation (15). Various thermophysical properties of the domains involved in the simulation are provided in Table 2.

For all domains, tetrahedral-shaped mesh was taken. In order to verify the irrelevance of the mesh and the simulation results, a single photovoltaic cell is investigated with three different mesh sizes at a laser beam divergence half-angle β of 0.001 rad and no rotation of the receiving end with respect to the laser irradiation direction and the laser power of 1 W. In Figure 6, comparing the short-circuit current I_{sc} at the receiving end of three sets of meshes, it was found that the difference in parameter values between the last two groups was relatively small. The second set of mesh is adopted.

3. Test and Platform for Regression

3.1. Test Setup. The general view of experimental setup is given in Figure 7. BWT Beijing DS3-51512 laser machine with function of adjusting power was taken for the test. The wavelength of the laser beam is 808 nm. Laser beam from this machine is directed to the square-shaped PV cell with 10 mm side. PV module in test is put inside the PMMA array or attached by glue to the PMMA base. The PV cell holder allows to adjust the system in different ways. It can be moved towards the laser and back, upward, and downward. It can be rotated to the 180 degree as well. All adjustments are smooth and accurate and allow to set up the position of the cell in space with high precision. The terminals of PV cell are connected to EKO I-V curve trace MP-160 by four wires: 2 wires are plugged to the positive terminal and 2 wires plugged to negative terminal of PV module. The I-V curve tracers measure the current and output the data by the wire to the PC. The data is processed by the software mp160i V2107.

3.2. Multivariable Regression. The unknown coefficients of multivariable regression C_1, C_2, and C_3 can be extracted by MATLAB program. Final regression results are presented in Table 3. According to the theory of multivariable regression, voltage is independent variable and current is dependent. The I-V curve is built by using Equation (11) including the coefficients of regression and other parameters.

The plot of experimental current against the fitted current calculated by using the equation $y = 0.9994 * x$ is built in order to prove the coefficient of determination R^2. It has well accuracy at $R^2 = 0.99$. Figure 8 includes eight curves with different intensity values from $2365.08\,\mathrm{W/m^2}$ to $3468.79\,\mathrm{W/m^2}$. The fit lines for each intensity with the special regression coefficients are added to Figure 9 as well.

4. Simulation Results and Analysis

In this part, three CPV systems with RTP concentrators of different heights (6 mm, 16 mm, and 25 mm) were studied to understand the impact of geometry on CPV performance. And the main impact of rotation angle was discussed.

4.1. Performance of Receiver Using RTP. The optical efficiency of the system was obtained by determining the number of rays that reached the PV cell surface and dividing it by the total number of rays. The light source remained fixed, while only the PV cell and concentrator were rotated. The measurement of optical efficiency was performed for RTP geometries with heights of 6 mm, 16 mm, and 25 mm, each of which was measured in the range from -70° to 70°, as shown in Figure 10. It illustrates that pyramids with heights of 16 mm and 25 mm exhibit very similar curves throughout

Table 2: Thermal properties of domains.

Domain	Material	Density (kg/m^3)	Heat capacity C_p (J/(kg•K))	Thermal conductivity k (W/(m•K))	Resistivity temperature coefficient a (1/K)	Thermal expansion α (1/K)
Concentrator	PMMA	1162	1465	0.1875	—	—
Busbar	Copper	8960	385	400	0.0039	$17 \cdot 10^{-6}$
Wafer	Silicon	2329	700	131	—	—
Fingers	Copper	8960	385	400	0.0039	$17 \cdot 10^{-6}$
Filling	Sylgard 165	1030	1046	0.16	—	—

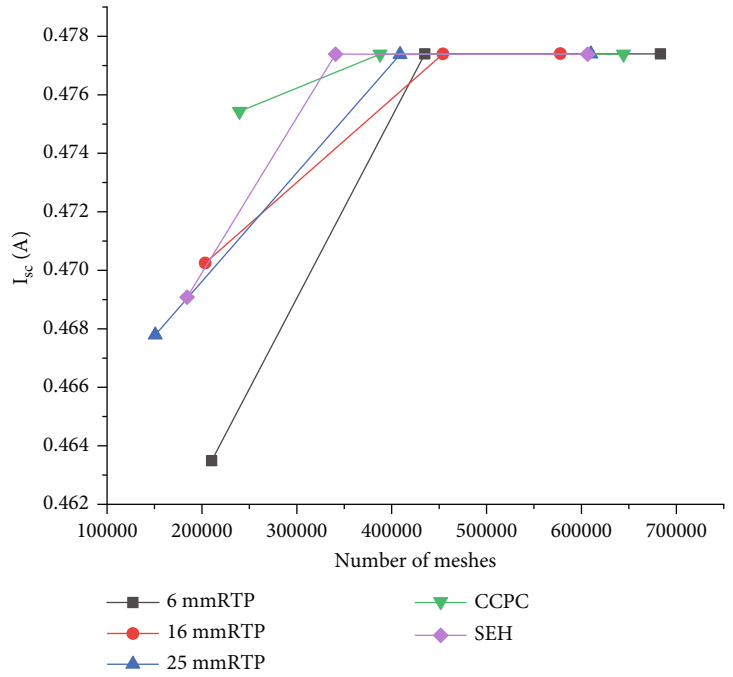

Figure 6: The short-circuit current I_{sc} at different mesh numbers.

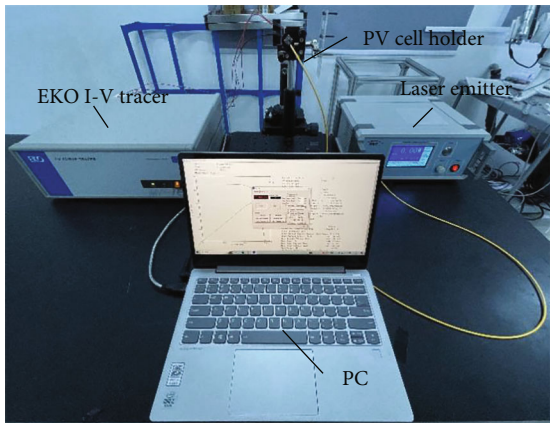

Figure 7: Arrangement of devices in test setup.

the entire range of measurements. Both of them achieve the highest efficiency, almost equal to 1, between -15° and 15°. However, as the angle increases beyond 15°, the efficiency drops dramatically, reaching close to zero at 45°. The 6 mm height pyramid shows a distinct behavior compared to the previous two. At 0° incidence, the efficiency is 0.88 because some rays reflect twice from the walls and escape from the concentrator. As the rotation angle increases, there is a slight decrease in efficiency, and it reaches zero at 70°.

The results clearly demonstrate that the height of the RTP concentrator significantly affects the performance of the PV cell, as the acceptance angle is directly dependent on the height while other parameters remain constant. The RTP with a height of 6 mm has the largest acceptance half-angle, equal to 37°. This geometry proves to be the most flexible in this study, as it is capable of accepting rays and maintaining relatively good efficiency across a wide range of angles. On the other hand, RTPs with heights of 16 mm and 25 mm do not exhibit such flexibility as the 6 mm height RTP, but they demonstrate near-perfect performance within a small range of angles.

The optical performance has been further confirmed by the heat flux sketches. As observed in Figure 11, all RTP concentrators exhibit relatively good uniformity in illumination distribution. The 6 mm RTP shows a slight increase in illumination from the sides towards the center. The 16 mm

Table 3: Final regression results.

C_1 (A/W)	C_2 (A/m^2•K^3)	C_3 (A/m^2•V)	R_s (ohm)	n (1)
7.05072*E*-05	-9312.94531	-0.026882943	0.21	1.65

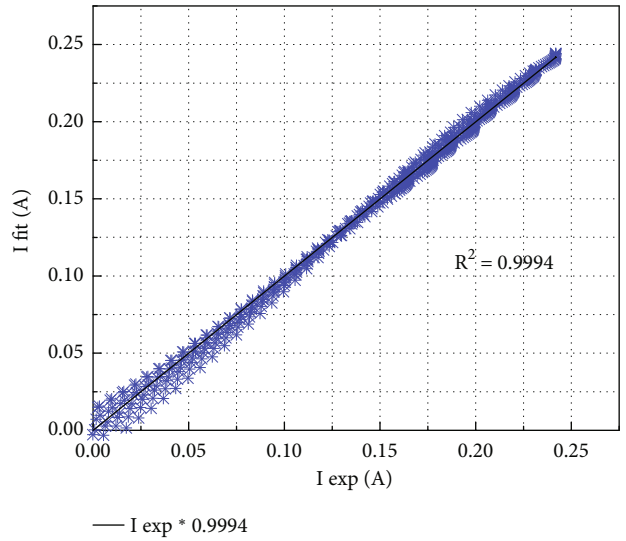

Figure 8: Coefficient of determination plot.

RTP displays the widest illumination distribution, while the peak value is greatest for the 25 mm RTP.

The temperature on PV panel in all the sketches is similar, but a trend of increasing temperature can be observed from the 6 mm RTP to the 25 mm RTP at the central zone of the PV surface, as Figure 12 shows. The difference between the peak temperatures of all PV cells does not exceed 1 K. The highest temperature is observed in the PV cell with the 25 mm RTP, reaching 321.19 K. The lowest temperature spot is at the corner of the CPV with the 6 mm RTP, where $T = 318.98$ K.

The simulated temperature of the entire CPV system is presented as a side view of the PV cell and RTP concentrator in Figure 13.The spots of the highest temperature ($T = 320$ K) and the lowest temperature ($T = 293$ K) are consistent in all the sketches. The variation in temperature distribution is due to the different dimensions of concentrators and their positions in space. The overall trend remains the same, with higher temperatures concentrated in certain areas and lower temperatures in other regions.

The rotation of CPV systems in space has a significant influence on the system's performance. In this study, different RTP concentrators were considered, and the main objective was to assess the efficiency drop caused by rotation and understand the main trends by comparing the different concentrators. Three RTP concentrators with heights of 6 mm, 16 mm, and 25 mm were investigated in this study. The optical, electrical, and thermal performance of these concentrators were measured at rotation angles of 0°, 10°, 30°, and 50°, while keeping other parameters constant. The overall results of efficiency and main trends are presented in Figure 14. In addition, the simulated heat flux and ray path of CPV with different RTP configurations are presented in Figure 15.

In Figure 14(a), the plot depicts the relationship between current, power, and voltage for the PV cell with the attached 6 mm pyramid concentrator. It is evident that the current curves at 0° and 10° rotation angles are very close, as are the two power curves at these angles. However, beyond 10° rotation, there is a significant drop in efficiency, reflected in the decreased current and power values. As the rotation angle increases further, there is a slight drop between 30° and 50°.

In Figure 14(b), the plot represents the current and power parameters for the CPV system with a 16 mm height RTP concentrator. Unlike the previous case, there is a significant drop observed between the current and power curves at 0°, 10°, and 30° rotation angles, and the absolute values of the current and power are lower compared to the 6 mm RTP. At 0° rotation, the highest I_{sc} value is 0.4774 A, while at 50° rotation, it drops to 0.269 A at 0 V. The peak power is $P = 0.2196$ W at 0.52 V and 0° and $P = 0.118$ W at 0.51 V and 50°. It is evident from Figures 15(a) and 15(b) that the heat flux distribution spot becomes less uniform and quickly moves towards the edge, and at 50°, no rays hit the PV cell. The peak heat flux values of the 16 mm RTP are lower at 0° ($2.09 \bullet 10^4 > 1.75 \bullet 10^4$ W/m^2) but slightly higher at 10° ($2.06 \bullet 10^4 > 1.97 \bullet 10^4$ W/m^2) compared to the 6 mm RTP. However, as the angle exceeds 30°, the peak heat flux starts to decrease and reaches 0 at 50°, indicating that the construction of the 16 mm RTP does not allow for effective ray collection at large rotation angles (30°, 50°) due to multiple reflections.

In Figure 14(c), the I-V and P-V data for the 25 mm RTP concentrator are presented. This geometry shows good performance, with differences compared to the 16 mm RTP only at 10° and 30° rotation angles, where the current and power values are slightly lower. The highest values of current and peak power are observed at 0°, with $I_{sc} = 0.4774$ A and $P = 0.2195$ W at 0.52 V, similar to the 6 mm and 16 mm RTP cases. The lowest values of I_{sc} and peak power are also the same as the 16 mm RTP, with $I_{sc} = 0.269$ A and $P = 0.118$ W at 0.51 V. As the rotation angle increases, the heat flux distribution becomes nonuniform, but the peak values at 10° ($2.97 \bullet 10^4$ W/m^2) and 30° ($3.67 \bullet 10^4$ W/m^2) are the highest among all pyramid concentrators. However, due to the small acceptance angle, this geometry has lower efficiency and becomes less effective at large rotation angles, as only a small number of rays hit the PV cell due to multiple reflections inside the concentrator.

At 0° rotation, the highest current value is $I_{sc} = 0.4774$ A at 0 V, and the peak power is $P = 0.2198$ W. At 50° rotation, the lowest current value is $I_{sc} = 0.401$ A, and the peak power is $P = 0.1826$ W. The gradual drop in efficiency can be attributed to the heat flux distribution, shown in Figure 15(a),

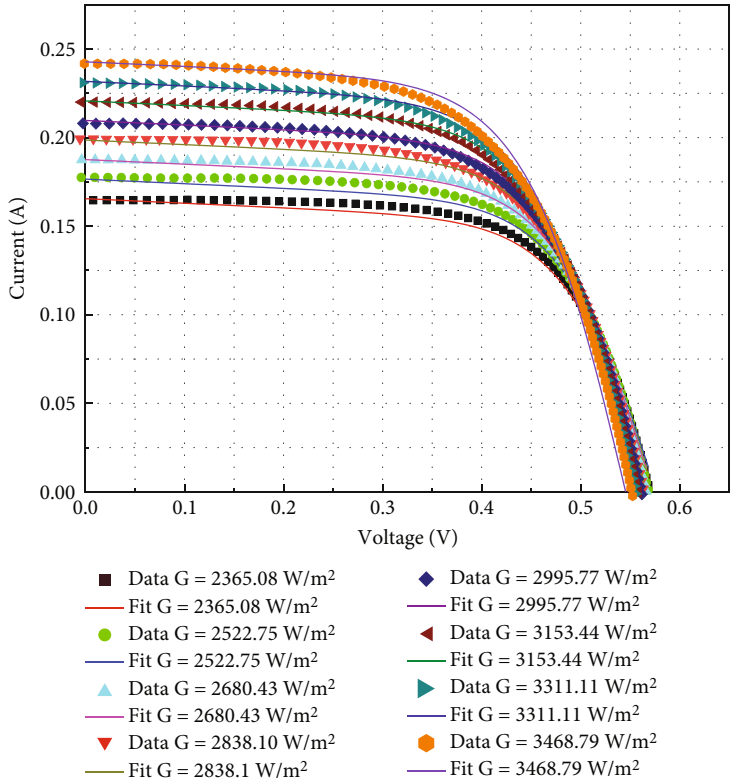

Figure 9: Experimental I-V curve trace and correspondent fitting with the same intensity and regression results.

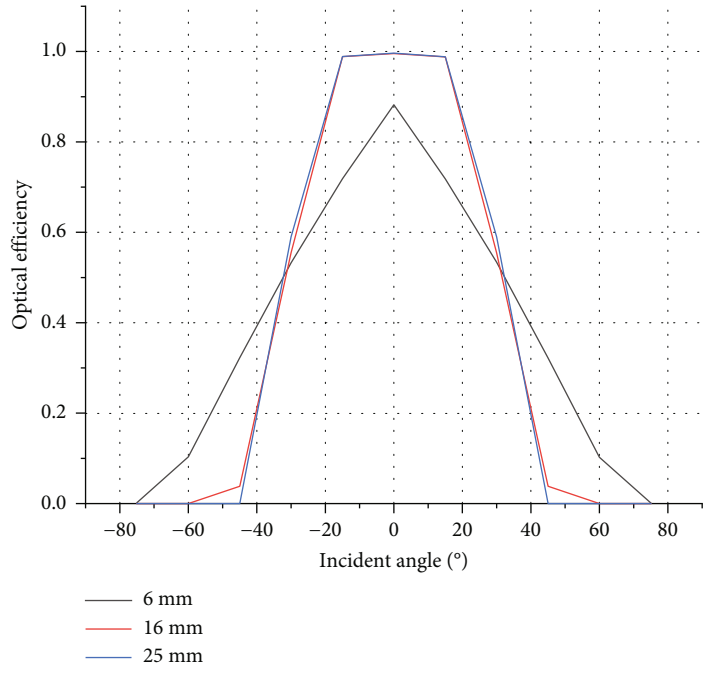

Figure 10: Simulated optical efficiency for different RTP.

where the peak illumination gradually shifts towards the edge of the PV cell. This observation is further confirmed by Figure 15(b), which shows the number of rays eventually hitting the PV cell. Despite the other RTP geometries, the 6 mm RTP with its large acceptance angle can collect rays even at a 50° rotation angle, resulting in an optical efficiency greater than 0. The peak value of heat flux at 0° rotation is $2.28 \bullet 10^4$ W/m^2.

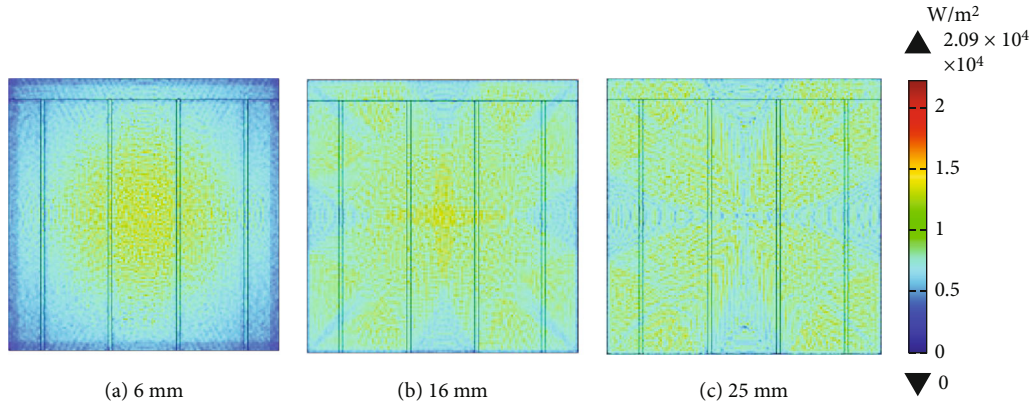

Figure 11: Simulated heat flux for CPV with different RTP.

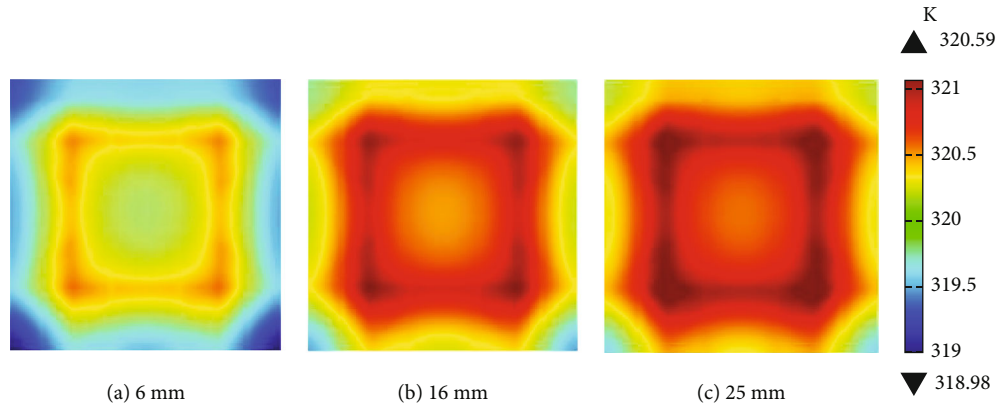

Figure 12: Simulated PV cell temperature for CPV with different RTP.

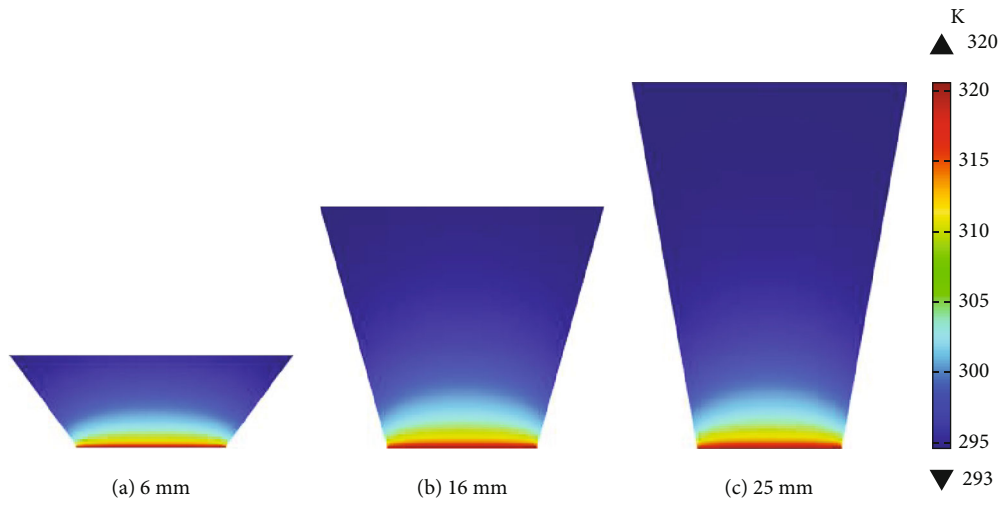

Figure 13: Simulated CPV system temperature for different RTP.

Figure 16 shows the current density and electric potential distributions, both of which depend on the illumination of the PV cell, which varies dramatically with rotation angle.

At 0° rotation, the current density distribution appears quite uniform, with the highest density spots located along the fingers and no shift of density towards the edges of the module. The highest peak value of current density is 15 A/m^2 for the 16 mm RTP, while the lowest is 14.2 A/m^2 for both the 6 mm and 25 mm RTP. The highest potential value is 0.61 V for all RTP.

As the rotation angle increases to 10°, the current density distribution changes. For the 6 mm RTP, the density shifts from the center to the edges, while for the 16 mm and 25 mm RTP, it shifts and concentrates at the center of the

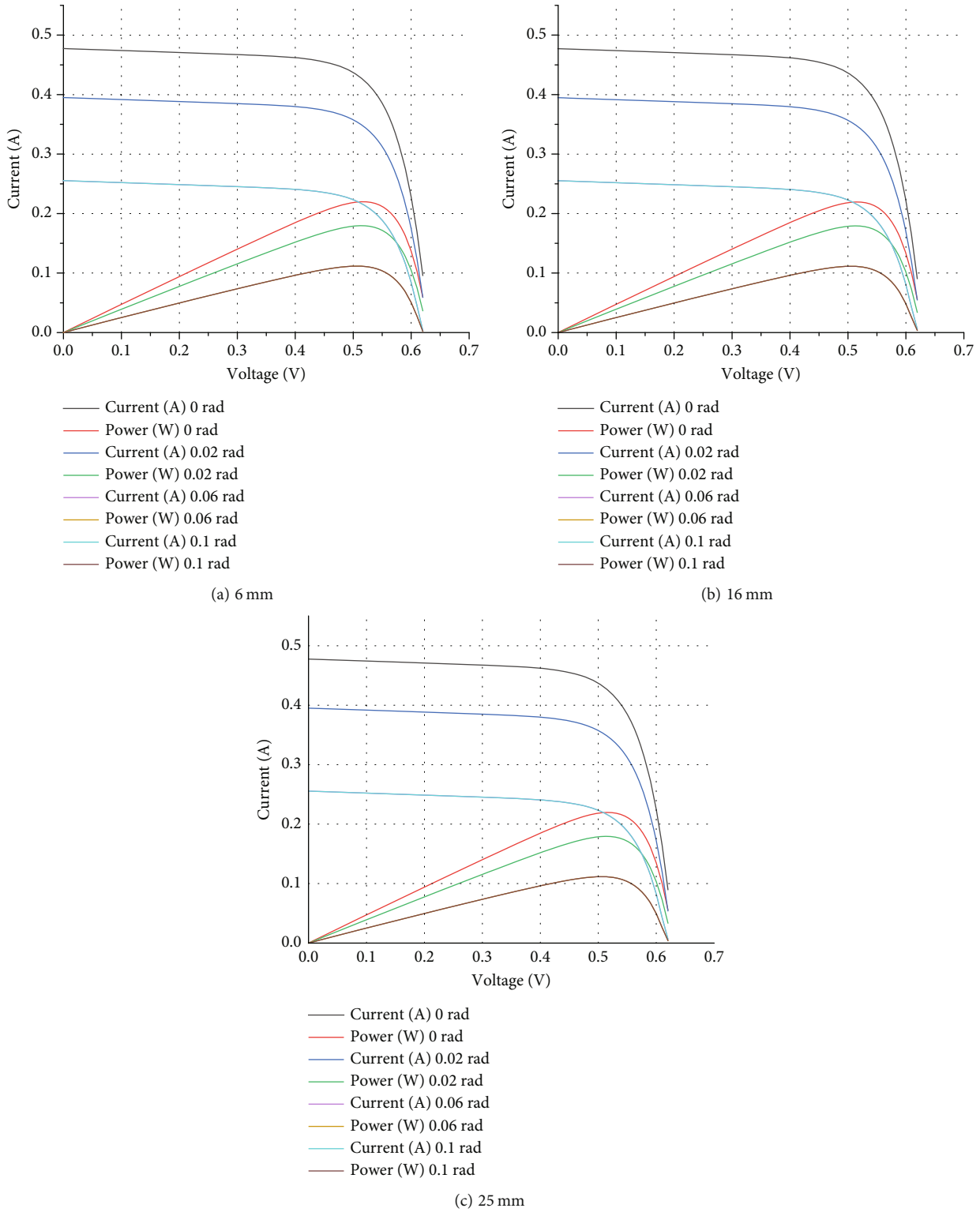

Figure 14: Simulated I-V and P-V curves of CPV with RTP of different height and rotation angles.

modules. The highest peak value of current density is 15.8 A/m^2 for the 6 mm RTP, while the lowest is 14.1 A/m^2 for the 25 mm RTP. The highest and lowest peak potentials are 0.62 V for the 6 mm RTP and 0.59 V for the 25 mm RTP, respectively.

At further increase in the angle to 30°, the higher density spot shifts to the center for the 6 mm RTP, while for the 16 mm RTP, the area of higher density strongly shifts to the side. The 25 mm RTP at this angle experiences a significant drop in peak density and voltage, having values of

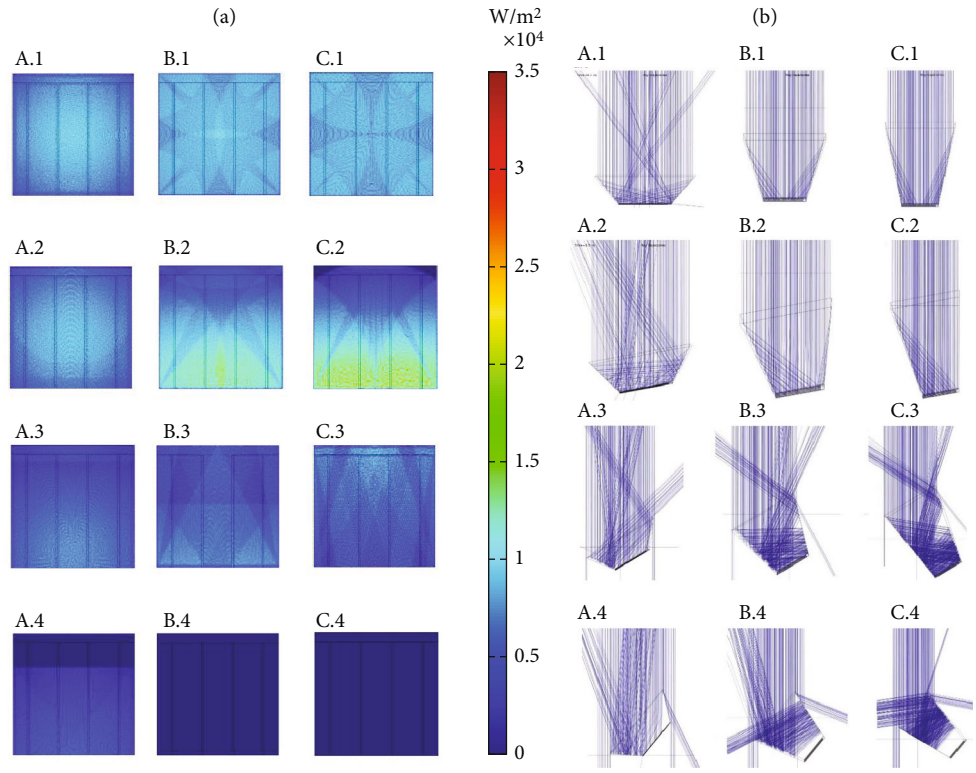

FIGURE 15: Simulated (a) heat flux and (b) ray traces of CPV with RTP of height (A) 6 mm, (B) 16 mm, and (C) 25 mm at rotation angles (1) 0°, (2) 10°, (3) 30, and (4) 50°.

8.75 A/m^2 and 0.33 V, respectively, which are the lowest among the considered concentrators. The highest performance is shown by the 6 mm RTP, with a current density of 14.9 A/m^2 and electric potential of 0.61 V.

At 50° rotation, only the 6 mm RTP shows relatively good efficiency, with a peak current density of 15.8 A/m^2 and a potential of 0.64 V. The other two concentrators have dramatically low values.

4.2. Performance Comparison of LWPT CPV Receivers with RTP, CCPC, and SEH. Throughout the detailed analysis conducted in the previous chapters, a vast amount of data encompassing thermal, electrical, and optical aspects has been thoroughly processed. The comparison of performance for each concentrator at perfect conditions is presented in Table 4. The conclusions drawn from this table clearly indicate that the RTP concentrator outperforms the other two concentrators in terms of output efficiency. It boasts higher values of power and current in comparison. Additionally, the fill factor, which serves as an important indicator of the CPV system's quality, is also superior for the RTP concentrator. These compelling results unequivocally demonstrate that the RTP lens represents the most efficient geometry at ideal conditions, even though its optical efficiency is lower than 100%. In summary, the study underscores the prominence of the RTP concentrator for achieving optimal efficiency and output performance in a CPV system under ideal conditions.

In Figure 17, the collected data of output power for each concentrator is displayed as the rotation angle is increased from 0° to 50°. Four measurements of power for each concentrator are shown at angles 0°, 10°, 30°, and 50°. The points representing each concentrator are differentiated by color and shape. The results clearly indicate that the RTP concentrator exhibits a significantly higher output power compared to the CCPC and SEH geometries, especially at angles greater than 0°. As the rotation angle increases, the difference in efficiency between the RTP and the other concentrators becomes even more pronounced, with the largest divergence observed at 50°. While the SEH shows slightly better efficiency at 30° compared to the CCPC, its performance at 0°, 10°, and 50° is similar to the CCPC. In conclusion, the RTP concentrator stands out as the most favorable choice for a CPV system that may be rotated in space relative to the laser beam, offering superior efficiency and output power performance. The RTP concentrator performs better when rotated for the following reasons: The RTP concentrator has a larger acceptance angle, which can collect more rays when the rotation angle is large and reflect collected light to the surface of the PV cell for the cell. In addition, the light is reflected several times from the inner surface of the RTP concentrator and is more evenly distributed on the surface of the PV cell, avoiding the problem of over heat, which also has a positive effect on the performance of the PV cell.

Figure 18 illustrates the most significant difference in electrical performance between the RTP, CCPC, and SEH

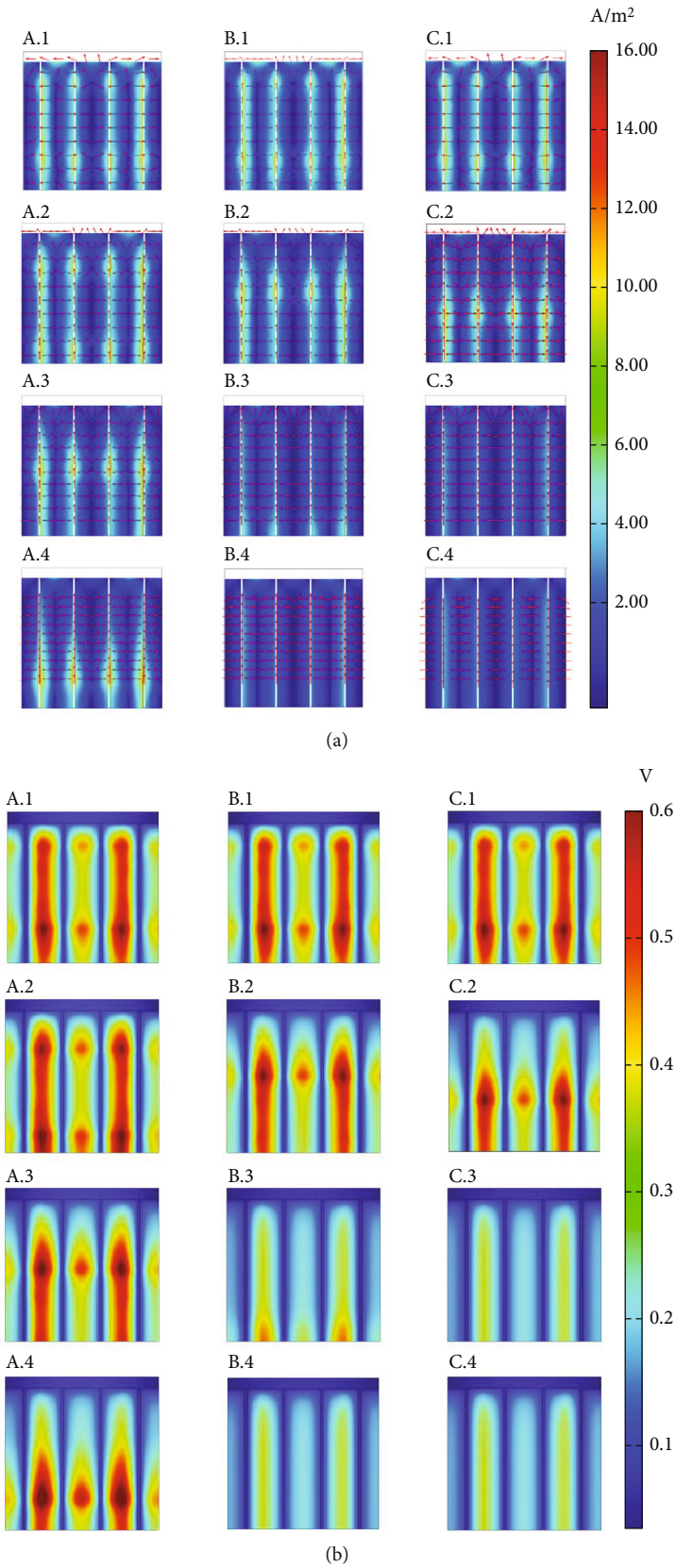

Figure 16: Simulated (a) current density and (b) electric potential of CPV with RTP of height (A) 6 mm, (B) 16 mm, and (C) 25 mm at rotation angles (1) 0°, (2) 10°, (3) 30°, and (4) 50°.

Table 4: Output parameters of different concentrators at perfect conditions.

Parameter	RTP	CCPC	SEH
V_{oc} (V)	0.63	0.63	0.63
I_{sc} (A)	0.4774	0.47739	0.47739
V_{mp} (V)	0.52	0.52	0.52
I_{mp} (A)	0.42276	0.42244	0.42198
P_m (W)	0.21983	0.21967	0.21943
FF (%)	0.7309	0.7304	0.7296
T_{max} (K)	320.59	320.88	321.31

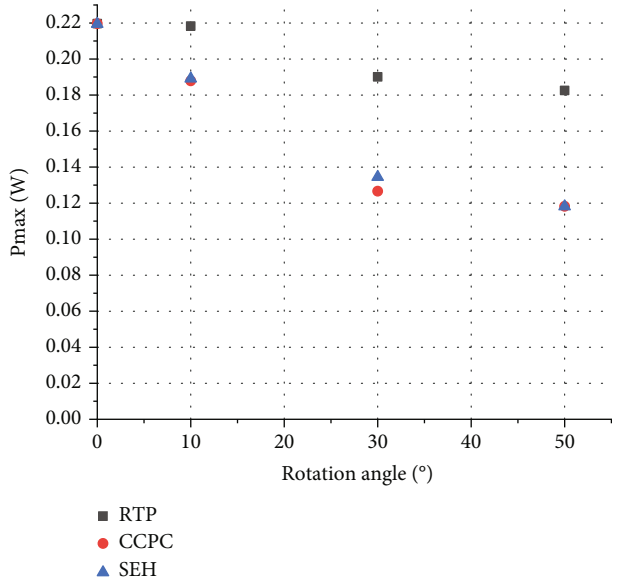

Figure 17: The performance comparison of different CPV with rotation.

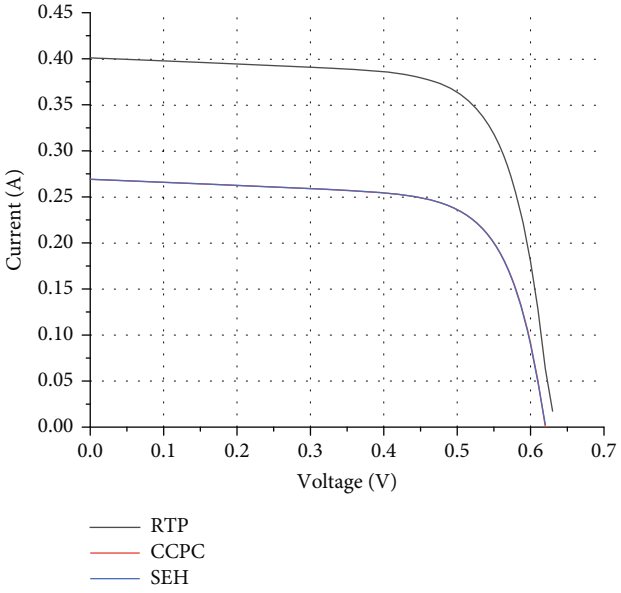

Figure 18: I-V data comparison at 50° rotation.

concentrators at a rotation angle of 50°. At this angle, the I_{sc} (short-circuit current) of the RTP concentrator is 0.4 A, while both the CCPC and SEH concentrators show very similar values, both around 0.27 A. The I-V curves further confirm the output power data depicted in Figure 17 and clearly demonstrate the superior performance of the RTP concentrator.

5. Conclusion

This research work focused on analyzing the multifield performance of LWPT receivers with nonimaging concentrators through simulation methods, using experimental data and regression coefficients obtained from tests. Different CPV systems with RTP, CCPC, and SEH concentrators were built and studied using FEM method. Three CPV systems with RTP concentrators of different heights (6 mm, 16 mm, and 25 mm) were studied to understand the impact of geometry on CPV performance. And the main impact of rotation angle was discussed. The results were presented in the form of plots and tables, showcasing the performance of the CPV systems under various parameters.

The simulation results clearly demonstrate that rotation factor significantly impacts the efficiency of power transmission in space or on Earth, particularly at long distances between emitter and receiver and small divergence angles of the laser. Among the RTP lenses, the 6 mm RTP shows promising optical and electrical performance, but further improvements are needed to enhance efficiency at shallow incidence angles. Comparing the conventional CCPC and sophisticated SEH with RTP, the CPV systems with RTP are even more efficient in certain cases.

Overall, this study provides valuable insights into the performance characteristics of different concentrator geometries in CPV systems, and the results suggest that RTP concentrators hold potential for efficient wireless power transmission using laser technology.

Data Availability

The data used to support the findings of this study are available from the corresponding author upon request.

Conflicts of Interest

The authors declare that they have no conflicts of interest.

Acknowledgments

This work was supported by the National Natural Science Foundation of China (No. 52176205 and No. U2241268) and the Innovation Capacity Support Plan in Shaanxi Province of China (Grant No. 2023-CX-TD-19).

References

[1] X. Zhu, K. Jin, Q. Hui, W. Gong, and D. Mao, "Long-range wireless microwave power transmission: a review of recent progress," *IEEE Journal of Emerging and Selected Topics in Power Electronics*, vol. 9, no. 4, pp. 4932–4946, 2021.

[2] K. Jin and W. Zhou, "Wireless laser power transmission: a review of recent progress," *IEEE Transactions on Power Electronics*, vol. 34, no. 4, pp. 3842–3859, 2019.

[3] P. Sprangle, B. Hafizi, A. Ting, and R. Fischer, "High-power lasers for directed-energy applications," *Applied Optics*, vol. 54, no. 31, pp. F201–F209, 2015.

[4] W. Li, L. Wu, and W. Wang, "Research progress of laser wireless power transmission," *Laser & Optoelectronics Progress*, vol. 55, no. 2, article 020008, 2018.

[5] L. Summerer and O. Purcell, *Concepts for wireless energy transmission via laser*, Europeans Space Agency (ESA)-Advanced Concepts Team, 2009.

[6] W. Zhou and K. Jin, "Power control method for improving efficiency of laser-based wireless power transmission system," *IET Power Electronics*, vol. 13, no. 10, pp. 2096–2105, 2020.

[7] G. Li, H. Zhang, C. Wang, and J. Lu, "Effect of 1070nm laser uniformity on temperature distribution and performance of In0. 3Ga0. 7As solar panel," in *Fifth International Symposium on Laser Interaction with Matter, Volume 11046*, pp. 109–117, Changsha, China, March 2019.

[8] H. Wang, J. Wang, H. Yang et al., "The effect of non-uniform irradiation on laser photovoltaics: experiments and simulations," *Photonics*, vol. 9, no. 7, p. 493, 2022.

[9] M. Xian-long, L. Bei, C. F. A. Lopez, and L. Cun-liang, "Multi-field coupling characteristics of photovoltaic cell under non-uniform laser beam irradiance," *Sustainable Energy Technologies and Assessments*, vol. 52, article 101963, 2022.

[10] C. E. Valdivia, M. M. Wilkins, S. S. Chahal et al., "Many-junction photovoltaic device performance under non-uniform high-concentration illumination," in *AIP Conference Proceedings, Volume 1881, Issue 1*, Ottawa, Canada, May 2017.

[11] M. El-Saftawy, A. M. Abd El-Hameed, and N. S. Khalifa, "Analytical studies of laser beam propagation through the atmosphere," in *Laser Science and Applications*, pp. 113–126, May 2010.

[12] S. P. Philipps, A. W. Bett, K. Horowitz, and S. Kurtz, *Current status of concentrator photovoltaic (CPV) technology*, National Renewable Energy Lab. (NREL), Golden, CO (United States), 2015.

[13] H. Elmustapha, T. Hoppe, and H. Bressers, "Comparing two pathways of strategic niche management in a developing economy; the cases of solar photovoltaic and solar thermal energy market development in Lebanon," *Journal of Cleaner Production*, vol. 186, pp. 155–167, 2018.

[14] S. P. Philipps and A. W. Bett, "III-V multi-junction solar cells and concentrating photovoltaic (CPV) systems," *Advanced Optical Technologies*, vol. 3, no. 5-6, pp. 469–478, 2014.

[15] E. F. Fernández, F. Almonacid, P. M. Rodrigo, and P. J. Pérez-Higueras, "CPV Systems," in *McEvoy's Handbook of Photovoltaics*, pp. 931–985, Academic Press, 2018.

[16] N. Sellami and T. K. Mallick, "Optical efficiency study of PV crossed compound parabolic concentrator," *Applied Energy*, vol. 102, pp. 868–876, 2013.

[17] M. Xian-long, H. Yi-chao, L. Bei, Z. Pu, C. Felipe Aristizabal Lopez, and L. Cun-liang, "Improvements of PV receiver in laser wireless power transmission by non-imaging optics," *Solar Energy*, vol. 255, pp. 157–170, 2023.

[18] L. O. Tamuno-Ibuomi, F. Muhammad-Sukki, R. Ramirez-Iniguez et al., "Indoor characterisation of a reverse truncated pyramid concentrator," in *2021 IEEE 48th photovoltaic specialists conference (PVSC)*, pp. 2348–2350, Fort Lauderdale, FL, USA, June 2021.

[19] M. Buljan, J. Mendes-Lopes, P. Benítez, and J. C. Miñano, "Recent trends in concentrated photovoltaics concentrators' architecture," *Journal of Photonics for Energy*, vol. 4, no. 1, pp. 040995–040995, 2014.

[20] J. P. Ferrer-Rodriguez, E. F. Fernandez, H. Baig, F. Almonacid, T. Mallick, and P. Perez-Higueras, "Development, indoor characterisation and comparison to optical modelling of four Fresnel-based high-CPV units equipped with refractive secondary optics," *Solar Energy Materials and Solar Cells*, vol. 186, pp. 273–283, 2018.

[21] V. Andreev, V. A. Grilikhes, V. P. Khvostikov et al., "Concentrator PV modules and solar cells for TPV systems," *Solar Energy Materials and Solar Cells*, vol. 84, no. 1-4, pp. 3–17, 2004.

[22] Q. Hu, Z. Li, L. Yang, K. Qiao, and X. Zhang, "Overview of research on space laser communication tracking and pointing technology," 2015.

[23] A. E. Siegman, *Lasers*, University science books, 1986.

[24] M. Wiesenfarth, I. Anton, and A. W. Bett, "Challenges in the design of concentrator photovoltaic (CPV) modules to achieve highest efficiencies," *Applied Physics Reviews*, vol. 5, no. 4, 2018.

[25] J. A. Nelson, *The Physics of Solar Cells*, World Scientific Publishing Company, 2003.

[26] J. A. Duffie and W. A. Beckman, *Solar Engineering of Thermal Processes*, John Wiley & Sons, 2013.